Bioinspired Underwater Navigation Using Polarization Patterns Within Snell's Window

CHENG Hao-yuan[a, b, *], YU Shi-min[a, b], YU Hao[c], ZHU Jin-chi[a, b], CHU Jin-kui[c]

[a] Department of Mechanical and Electrical Engineering, Ocean University of China, Qingdao 266100, China

[b] Key Laboratory of Ocean Engineering of Shandong Province, Ocean University of China, Qingdao 266100, China

[c] Key Laboratory for Micro/Nano Technology and System of Liaoning Province, Dalian University of Technology, Dalian 116024, China

Abstract

Aiming at the requirement of autonomous navigation capability of the underwater unmanned vehicle (UUV), a novel bionic method for underwater navigation based on polarization pattern within Snell's window is proposed. Inspired by creatures, polarization navigation is a satellite-free navigation scheme and has great potential to be used in the water. However, because of the complex underwater environment, whether UUV polarization navigation can be realized is doubtful. To illustrate the feasibility of underwater polarization navigation, we firstly establish the model of underwater polarization patterns to prove the stability and predictability of the underwater polarization pattern within Snell's window. Then, we carry out static and dynamic experiments of underwater heading determination based on developed polarization information detection equipment. Finally, we obtain underwater polarization patterns and conduct the tracking experiment at different water depths. The experimental results of the underwater polarization patterns are consistent with the simulation, which proves the correctness of the proposed model. At the water depth of 5 m, the average angle and position error of the tracking experiment are 14.3508° and 4.0812 m, respectively. It is illustrated that underwater polarization navigation is realizable and the precision can meet the real-time navigation requirements of UUV. This study promotes the improvement of underwater navigation ability and the development of marine equipment.

Key words: underwater navigation, polarization pattern, heading determination, tracking experiment

---

1 Introduction

The ocean area of the earth is vast and there are still a large number of sea areas to be explored and exploited. Therefore, UUV has become an important platform for ocean exploration. It plays an important role in safety search and rescue, pipeline inspection, ocean detection, underwater archaeology, and aquaculture. Due to the particularity of the working environment, UUV needs longtime underwater diving and standby, which puts forward higher requirements for underwater navigation technology (Miller et al., 2010). Various methods were developed to improve underwater navigation ability, but they all have some drawbacks. The global navigation satellite system is hard to be used underwater in deep water because of the rapid attenuation of radio signals (Paull et al., 2014). The attitude error obtained by the inertial navigation system accumulates over time (Stutters et al., 2008). The geomagnetic navigation system cannot work in uncertain magnetic fields (Wu et al., 2018). Therefore, it is necessary to develop a new navigation system that does not rely on satellite navigation and can effectively improve inertial navigation. This new navigation technology needs to have comprehensive advantages in cost, coverage, accuracy, anti-interference, and viability.

Physicists have found that after undergoing atmospheric scattering, air-water interface refraction, and underwater scattering, sunlight eventually forms a particular pattern of underwater polarization. When viewed upward from calm water, the field of view above the water surface is compressed to a conical area of approximately 97.5° due to the refraction effect. This field of view is called Snell's window. The polarization pattern in Snell's window under a calm water surface is usually relatively stable under certain conditions and contains important orientation information, which can be used by underwater organisms and even humans. It has

been proven that polarization has great superiority in the water (Cheng et al., 2021b; Zhang et al., 2021). Many creatures have evolved for millions of years and natural selection has given them many navigational skills. In the water, a variety of creatures can use polarization for navigation, predation, disguise, and communication (Shashar et al., 2000; Waterman, 2006; Cartron et al., 2013). Among them, a grass shrimp named Palaemonetes vulgaris (Goddard and Forward, 1991; Horváth and Varjú, 1995) can perceive the underwater polarization pattern in Snell's window and uses this pattern as a direction cue to move away from the coastline predators. In the process of migration, rainbow trout (Hawryshyn and Bolger, 1990; Browman and Hawryshyn, 1994; Parkyn et al., 2003) can make use of underwater polarization patterns to realize navigation. The vision system of mantis shrimp (Bok et al., 2014; Gagnon et al., 2015) can detect and analyze visible light, ultraviolet light, linearly and circularly polarized light, which enables it to accurately capture prey, avoid natural enemies, and even navigate in the underwater environment with low illumination, strong scattering, and high turbidity. All these results prove the feasibility of underwater polarization navigation. Bionic navigation has great autonomy because all the information required is from nature. In addition, as an information carrier, the information of polarized light is more robust than the light intensity information in the underwater environment with low illumination and high scattering. Inspired by creatures that have polarization sensitivity, a bionic polarized optical guidance system (Cheng et al., 2020b) was developed for underwater vehicle docking. Bionic polarization navigation is a new technology that has the potential to be applied in water. If underwater polarization navigation technology is developed further, new ideas will be provided for underwater navigation. To realize underwater polarization navigation, the study of underwater polarization patterns is necessary. Sabbah et al. (2006) used the Mueller matrix and Stokes vector to simulate the underwater polarization distribution considering the refraction of the air-water interface. Then, the effect of wavy water surface (Zhou et al., 2017), water molecules (Cheng et al., 2020a), suspended particles (Cheng et al., 2020c), and other various factors (Cheng et al., 2021a) on the underwater polarization patterns were studied. At the same time, researchers have conducted some proof-of-concept studies of underwater polarization navigation (Powell et al., 2018). It is preliminarily illustrated that underwater polarization patterns can be used to navigate but specific underwater navigation experiment based on the UUV is lacking.

To further improve the working performance and survivability of UUV, this paper focuses on the underwater navigation technical requirements of long-term, autonomous, high-precision, and high-concealment. By imitating the underwater organism function of sensing polarized light for navigation, we propose a method for UUV navigation based on underwater polarization patterns. First, using the Stokes vector and Mueller matrix, the model of underwater polarization pattern is established considering atmospheric polarization patterns, surface refraction, and underwater scattering. For clear water, the scattering of water molecules is described by the single Rayleigh scattering model. For turbidity water, the scattering of suspended particles is described based on the combination of Monte Carlo simulation and Mie scattering theory. Next, by mimicking the polarization-sensitive structure and mechanism of underwater organisms, we develop the underwater polarization information detection equipment and build it on the ROV (Remote operated vehicle). Based on the developed device, the static and dynamic experiments of heading determination in the water tank are carried out. Finally, in real underwater environments, we obtain underwater polarization patterns to prove the correctness of the model and conduct the underwater tracking experiment. The results show that underwater polarization navigation is feasible and it will be a great complement to underwater navigation.

2 Theory

2.1 Underwater polarization patterns

To realize underwater polarization navigation, we need to establish the model of underwater polarization patterns. When sunlight enters the water from the atmosphere, it is scattered by the atmospheric molecules and aerosols, refracted by the air-water interface, and further scattered by the underwater particles, as shown in Fig. 1. This process produces underwater polarization patterns, which are also useful for the retrieval of marine particles (Liu et al., 2020), target detection (Tian et al., 2018), and image recovery (Huang et al., 2016). In this paper, we describe underwater polarization patterns by the degree of polarization (DOP) and angle of polarization (AOP). The Stokes vector and Mueller matrix are used to simulate the underwater polarization pattern.

Atmospheric polarized light can be described by the Stokes vector $S = [I, Q, U, V]^T$, which contains all informa-
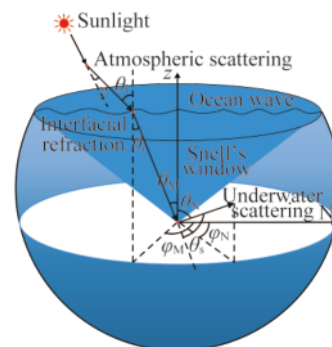

Fig. 1. Atmosphere-ocean optics.

tion of polarized light. I is the total intensity of light, Q quantifies the fraction of linear polarization parallel to a reference plane, U gives the proportion of linear polarization at 45° to the reference plane, and V describes the fraction of right-handed circular polarization. The Stokes vector form of incident light can be written as follows:

$$S_i = \begin{bmatrix} 1 \\ P\cos 2\psi \\ P\sin 2\psi \\ 0 \end{bmatrix}, \tag{1}$$

where P and ψ are the atmospheric DOP and AOP, respectively. DOP ranges from 0 to 100%. AOP is defined to vary from −90° to 90°. AOP is the current orientation to the max polarity direction of polarized light. Because of its stability, AOP is always used to determine the heading angle in skylight navigation (Dupeyroux et al., 2019). According to the Rayleigh atmosphere model, the skylight polarization pattern can be expressed as:

$$P = P_{max}\frac{\sin^2\gamma}{1+\cos^2\gamma}; \tag{2}$$

$$\tan\psi = \frac{\sin\theta_N\cos\theta_M - \cos\theta_N\cos(\phi_N-\phi_M)\sin\theta_M}{\sin(\phi_N-\phi_M)\sin\theta_M}. \tag{3}$$

where, P_{max} must be measured and is made equal to unity here for simplicity. Atmospheric scattering angle γ is the angle between the observed and incident direction. θ_M and θ_N are atmospheric zenith angles of the sun and observation, respectively. ϕ_M and ϕ_N are atmospheric azimuth angles of the sun and observation, respectively.

The air−water interface refraction of skylight is described by the Mueller matrix:

$$M_r = \frac{\sin 2\theta_i / \sin 2\theta_r}{2\sin^2\theta_1/\cos^2\theta_2} \times$$

$$\begin{bmatrix} \cos^2\theta_2+1 & \cos^2\theta_2-1 & 0 & 0 \\ \cos^2\theta_2-1 & \cos^2\theta_2+1 & 0 & 0 \\ 0 & 0 & 2\cos\theta_2 & 0 \\ 0 & 0 & 0 & 2\cos\theta_2 \end{bmatrix}. \tag{4}$$

Incident angle θ_i is the vertical angle between the incident light and the zenith. Refraction angle θ_r is the vertical angle between the refracted light and the zenith. $\theta_1=\theta_i+\theta_r$ and $\theta_2=\theta_i-\theta_r$. Considering the presence of waves in the real ocean, we also improve the refraction model by adding the Cox−Munk ocean wave model (Cox and Munk, 1954), which is a function of wind speed and direction.

The influence of particle scattering on underwater polarization patterns is great. When the water quality is good, underwater polarization patterns mainly depend on the single Rayleigh scattering of water molecules (Cheng et al., 2020b) because they are the most abundant constituent in clear water. The Mueller matrix of underwater Rayleigh scattering is:

$$M_R(\theta_s) = \frac{3(1-\rho)}{4(1+\rho/2)} \times$$

$$\begin{bmatrix} \dfrac{1+\rho}{1-\rho}+\cos^2\theta_s & -\sin^2\theta_s & 0 & 0 \\ -\sin^2\theta_s & 1+\cos^2\theta_s & 0 & 0 \\ 0 & 0 & 2\cos\theta_s & 0 \\ 0 & 0 & 0 & \dfrac{2-4\rho}{1-\rho}\cos\theta_s \end{bmatrix}. \tag{5}$$

where, underwater scattering angle angle θ_s is the angle between the refracted and scattered light. ρ is the depolarization factor. Clear underwater scattering Mueller matrix is:

$$M_S = R(\sigma_2)M_R(\theta_s)R(\sigma_1). \tag{6}$$

The rotation matrix $R(\sigma)$ is required to change the plane of reference when the viewing direction is not in the principal plane (You et al., 2011). The rotation angles σ_1 and σ_2 are related to the incident and scattered directions.

We use multiple Mie scattering and Monte Carlo model (Cheng et al., 2020c) to describe the underwater scattering of suspended particles when the water quality is poor. The multiple Mie scattering Mueller matrix of turbid water is shown below:

$$M_S = \prod_{k=0}^{k'} R_k(\sigma_2)M_k(\theta_s)R_k(\sigma_1), \tag{7}$$

where k is the scattering number. The single Mie scattering Mueller matrix $M_k(\theta_s)$ can be confirmed by Mie theory.

The final Stokes vector $S_f = [I',Q',U',V']^T$ is:

$$S_f = M_S M_r S_i. \tag{8}$$

Then the underwater DOP P' and AOP ψ' are solved:

$$P' = \frac{\sqrt{Q'^2+U'^2}}{I'}; \tag{9}$$

$$\psi' = \frac{1}{2}\arctan\left(\frac{U'}{Q'}\right). \tag{10}$$

2.2 Underwater polarization navigation

The underwater AOP pattern obtained by the polarization imaging technique represents the direction of the polarization electric vector. It is distributed on both sides of the solar meridian in a symmetric pattern. The AOP at any geographic location is only related to the sun altitude angle, sun azimuth angle, observed altitude angle, and observed azimuth angle, and is not affected by other factors. Therefore, when the position of the sun is known at any time after the space position is determined, the polarization pattern of the sky at the location is stable, which provides a stable information source for the use of the polarized light field for navigation and orientation. DOP and AOP distributions have obvious data patterns at any time, so the solar meridian can be used as an angle reference for heading measurement.

The specific steps to obtain the position of the sun meridian are as follows. Based on the Stokes vector princi-

ple, the AOP patterns can be obtained by polarization camera and coordinate transformation. Different azimuth values of polarization can be distinguished by pixel values. The characteristic region of the solar meridian has an obvious edge, which shows a significant mutation of the gray value in image processing. We can acquire the characteristic region of the solar meridian by setting the characteristic threshold value. Next, we detect the edge of the characteristic region of the solar meridian based on the Canny operator. The azimuth of the solar meridian is obtained by using the Hough transform and symmetry distribution relation (Fig. 2). Then, we can calculate the heading angle by combining the north finder data.
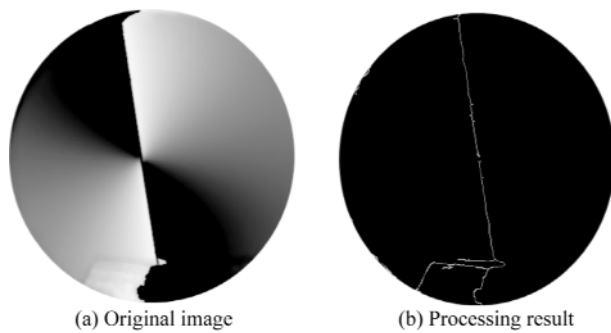

(a) Original image   (b) Processing result

Fig. 2. Solar meridian extraction results.

In this way, we obtain polarization navigation data through the AOP pattern. The azimuth of the polarization or the direction of the solar meridian obtained by the polarization detection method can determine the reference angle between the carrier axis and solar meridian, which is the relative angle. The angle between the body axis and the true north can be obtained by means of compass-assisted orientation, namely, the course angle of the carrier.

3 Heading determination

For autonomous navigation of UUV, any sensor error will affect the navigation accuracy. The influence of heading error is prominent, which will make the vehicle deviate from the course and cause the accumulation of position errors. Polarization patterns can provide UUV with heading information and effectively improve navigation accuracy because it has no error accumulation in measurement and strong anti-interference ability (Wang et al., 2015). In order to verify the feasibility of underwater polarization navigation, the static and dynamic experiments of heading determination based on underwater polarization patterns were carried out in the late afternoon. The weather was clear without clouds and the wind speed was low.

Fig. 3 shows the static experiment of underwater heading determination. There is no displacement in the experiment, so it is called the static experiment. After the water tank was filled with clean water, an electric turntable drove the polarization camera to rotate at a speed of 5°/s and we recorded data every 5°. The size of the tank is 1.7 m×1.7 m×0.7 m, and there is an observation hole at the bottom for the polarization camera to observe the underwater polarization pattern induced by water surface refraction and underwater particle scattering. The electric turntable, whose accuracy is 0.001°, was used to rotate the polarization camera and calculate relevant angle error. The division of the focal plane polarization camera (LUCID, PHX050S-P) can take four images at different polarization angles at once to calculate the polarization information. It has 2448×2048 pixels and the physical size of every pixel is 3.45 μm. We corrected the distortion of the images induced by the seawater, fisheye lens, and waterproof cover (Zhang, 2000). The north seeker can accurately find the north within the range of attitude angle ±7° and has the characteristics of the fast start and high north finding accuracy. Its technical parameters are shown in Table 1. The navigation information was obtained by the correlation algorithm based on the Hough transform (Section 2.2) after the polarization pattern was captured by the polarization camera.

The corresponding solar azimuth angle can be calculated by the astronomical almanac, and then the experimental error can be obtained. Fig. 4 shows the comparison between the solar azimuth measured by the polarization camera rotating 360° and the theoretical value. The average heading error is 0.3954°. In the static experiment, the attitude of the
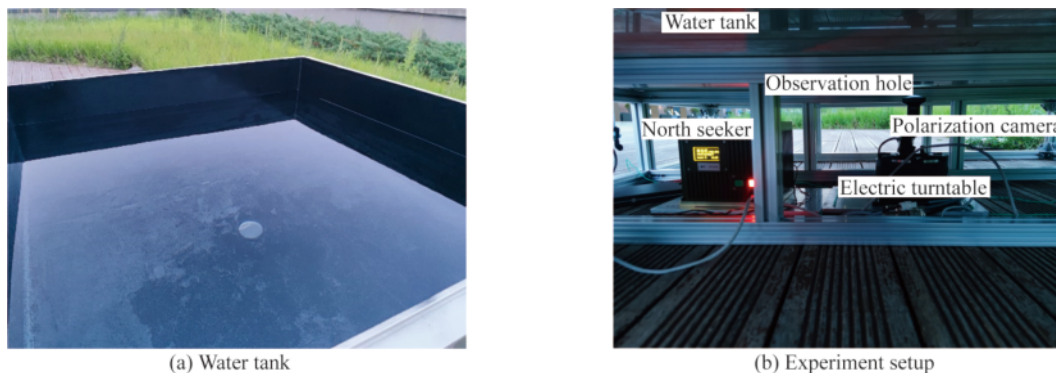

(a) Water tank

(b) Experiment setup

Fig. 3. Static experiment of underwater heading determination.

Table 1 North seeker parameters

Parameter	Value
Measuring range	0°−360°
Precision	Smaller than 1°
Start-up time	10 s
North seek time	3 min/5 min
Supply district	+9−+36 V DC
Maxim power consumption	30 W

polarization camera is stable and other interference factors are controllable. Thus, the angle error is small and the results preliminarily verify the feasibility of the method.

In the dynamic experiment, the heading information of the vehicle was recorded through the inertial sensor, and the specific parameters are shown in Table 2. The sensor is a small, GPS-free inertial measurement unit weighing just 55 g for a variety of guidance and navigation applications. Three inclinometers are built in to ensure accurate system leveling and an external synchronization signal input is provided. The applications of the sensor include inertial navigation research and production, weapon system guidance and control, mobile mapping platform attitude measurement, unmanned equipment control, and aerospace equipment attitude measurement control. The polarization camera, inertial sensor, and mobile power supply were waterproof, as shown in Fig. 5a, and built on ROV, as shown in Fig. 5b. The ROV (parameters shown in Table 3) is a typical open-frame structure, consisting of two compartments, namely power and electronic compartments, with six thrusters in total. Solid buoyancy material and lead weight are located at the uppermost and lowermost parts, respectively. The hardware part mainly includes the ground station (remote control and computer), ROV, and umbilical cable. It can realize the cen-

Table 2 Inertial sensor parameters

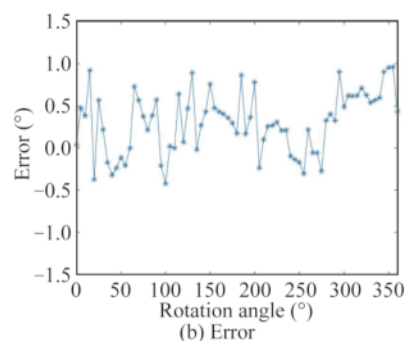| Parameter	Value
Size	44.8 mm×38.6 mm×21.5 mm
Working voltage	5 V±0.5 V
Sampling rate	2000 Hz
Measuring range	±400 °/s
Gyro bias instability	0.5 °/h
Resolution ratio	0.22 °/h
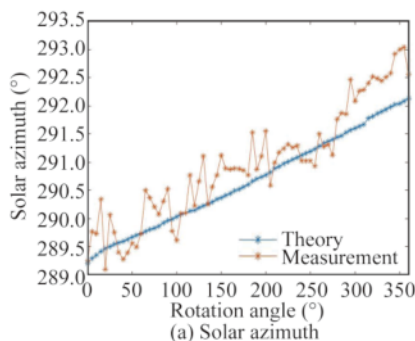
timeter depth control and automatically maintain a navigation lock without operating instructions by default. This ROV, which has the accurate feedback control and stable attitude, is widely used in underwater observation and exploration, marine equipment inspection, water sampling and measurement, and other fields. Fig. 5c shows the dynamic experiment in the water tank. The ROV was controlled to drive a certain trajectory smoothly at a uniform speed underwater and the relevant data obtained by the polarization camera and inertial sensor were recorded during the process.

Fig. 6 shows the comparison between the calculated data and the theoretical values. The average heading error is 0.8268°. Due to the movement of the ROV, there were some waves on the water surface, and the attitude of the polarization camera was unstable. All of these have a negative influence on the underwater polarization patterns, which leads to a decrease in accuracy. However, the underwater heading determination based on polarization patterns is feasible. The research lays a foundation for the tracking experiment in real underwater experiments.

4 Tracking experiment

With the increasing complexity of underwater tasks, a single sensor can no longer meet the requirements of navigation accuracy. Therefore, it is necessary to process and fuse the information of multiple sensors to accurately estimate the state of UUV. The fusion of multi-sensor information can not only increase the confidence of data and improve the fault tolerance of navigation, but also help to reduce the performance requirements of a single sensor and improve the speed of information processing. In order to realize the underwater location, based on the polarization camera and inertial sensor, an intelligent navigation method combining multi-source information (polarization and inertia) was constructed. The system uses the navigation coordinate system as the local horizontal coordinate system. In the acceleration integral loop, gravity acceleration and Coriolis acceleration are first calculated based on the position information in the initial calibration. Then, the observed specific force vector is converted to the navigation coordinate system by using the direction cosine matrix information. The position coor-

(a) Solar azimuth

(b) Error

Fig. 4. Static experiment results of underwater heading determination.
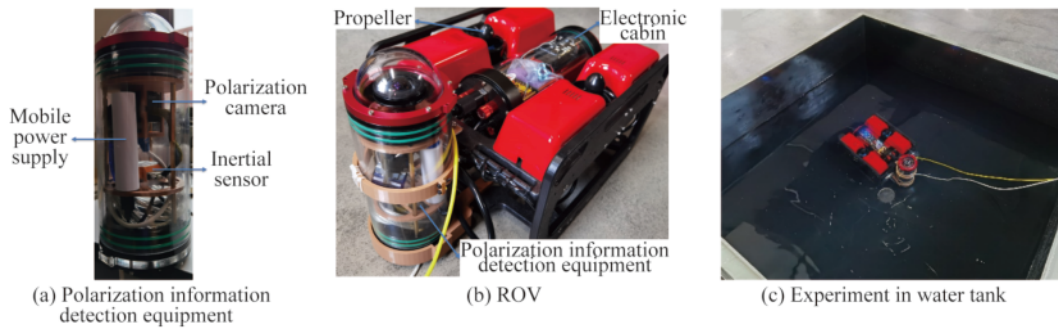
Fig. 5. Dynamic experiment of underwater heading determination.

Table 3　ROV parameters

Parameter	Value
Size	38 cm×33 cm×22 cm
Maximum depth	150 m
Speed	0.5−1 m/s
Single propeller thrust	1−3 kg
Maximum current of electrical adjustment	30 A

dinates are obtained by two integrations successively with Coriolis correction and gravity correction. In the angular velocity integral loop, to obtain the rotation angular velocity of the carrier coordinate system relative to the navigation coordinate system, the navigation information (position and velocity) output by the acceleration integral loop needs to be fed back to the angular velocity integral loop, so as to calculate the angular velocity value of the navigation coordinate system caused by the carrier movement and the earth rotation. Next, we can convert the angular velocity vector of the observed carrier relative to the inertial coordinate system into the angular velocity vector of the carrier relative to the navigation coordinate system, so as to update the direction cosine matrix. The difference between the output heading angle of the polarization and inertial information is used as the measurement value of the Kalman filter to correct the accumulated error of the inertial navigation system by the polarization navigation information. The modified direction cosine matrix is involved in the acceleration integration loop, thus indirectly correcting the position and velocity information of the system.

The angle and position obtained by the system were recorded and compared with the Global positioning system (GPS) navigation information to obtain the system's accuracy and verify the feasibility of underwater polarization navigation. The underwater positioning system (Fig. 7) is mainly composed of two parts: the ground station and the underwater experiment device. The transmitter and receiver are used to receive ground signals to unlock the device. The digital radio is used to realize information interaction with the ground station. The control system is used to receive and process the information of each sensor in real time. The polarization camera is used to obtain underwater polarization information. The MPU 6000 inertial sensor (131 LSB/(°/s); 4096 LSB/g) integrated into the control system is used to calculate the angle and position information. It is composed of a three-axis gyroscope and a three-axis accelerometer. The GPS positioning module can obtain real-time geographic location information to verify the accuracy of the underwater polarization navigation. The GPS module selected in this paper is NEO-M8N (2 m CEP), which has the characteristics of good stability, high accuracy, and fast update frequency, and can meet the experimental requirements. The information of specific force and angular velocity output by the inertial sensor was collected and compensated. The ROV heading, pitch, roll, speed, and position were obtained according to the mathematical model of the strapdown inertial navigation system. With the aid of the polarization navigation information, the Kalman filter method was used to estimate the nav-
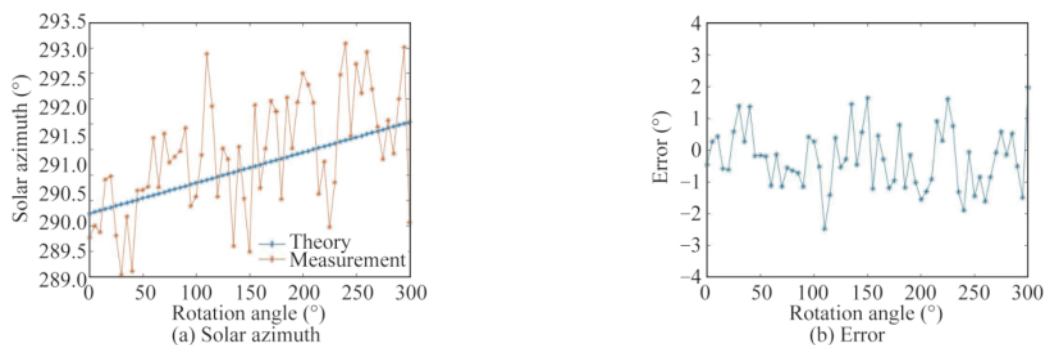

Fig. 6.　Dynamic experiment results of underwater heading determination.
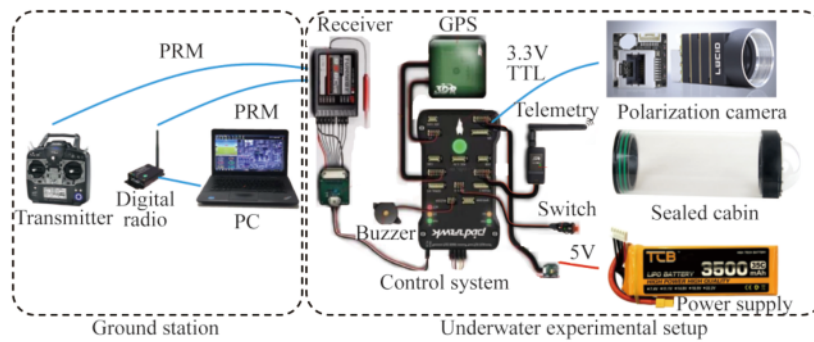
Fig. 7. Positioning system of underwater tracking experiment.

igation error of the strapdown system and compensate for it to get the optimal navigation structure of attitude, speed, and position.

　　Whether polarization navigation technology can be realized underwater depends on the stability of detected underwater polarization patterns. If the polarization pattern, such as DOP or AOP, is robust in the general underwater environment, the navigation information contained in the pattern can be obtained by image processing to realize underwater polarization navigation. To prove that underwater polarization patterns are regular and further serve for underwater navigation, we captured the underwater polarization patterns at different time (Fig. 8) and depths (Fig. 9) in the real underwater environment. The underwater experiment was performed under clear weather conditions at a depth of 1 m, 3 m, and 5 m. The wind was southeast and the speed was about 5 m/s. There were some waves on the surface of the ocean. The underwater environment in the experiment was complex. The water was semi-turbid and the visibility was
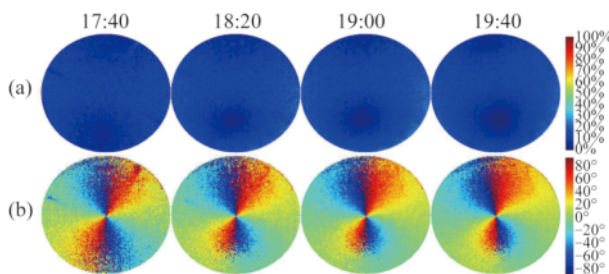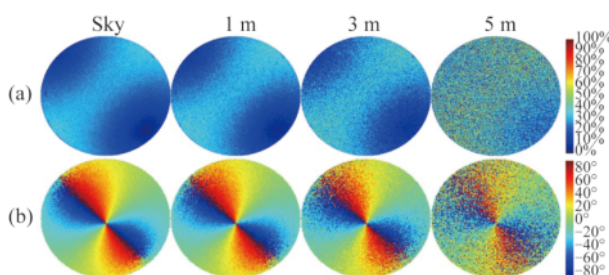
poor owing to the absorption and scattering of light by various particles. The ocean wave, shoreline, seabed, and waterproof device had a negative influence on the experiment due to their impacts on the light. The maximum DOP occurs at sunrise and sunset (Cheng et al., 2020b), and thus we experimented within this time range. We used a long exposure time to overcome the low light in the water. Experimental results show that underwater polarization patterns are regular and the navigation based on them is realizable. Underwater polarization patterns within Snell's window, whose main affecting factor is the sun position, are stable and similar to atmospheric polarization patterns. Underwater light is partially polarized except for the neutral points. The DOP is concentric around the sun position and symmetrical about the solar principal plane. The AOP is negative about the solar principal plane and keeps the robustness in most cases. However, polarization patterns cannot be maintained at deep water because there is an increase in multiple scattering. At deep waters, polarization characteristics cannot be maintained (Shashar et al., 2004). Snell's window is dark and shows no apparent color or structure (Lynch, 2015). With depth increase, the effect of sun position on both the DOP (Ivanoff and Waterman, 1958) and AOP (Waterman, 1955) diminishes. Although there are some noisy points in the patterns and the DOP value is low, we can still distinguish the patterns, especially AOP. It proves the feasibility of underwater polarization navigation. Thus, we choose AOP patterns within Snell's window to conduct the navigation.

　　After proving the regularity of underwater polarization patterns, we conducted the underwater tracking experiment and realize underwater positioning. We controlled the ROV to move horizontally so that the polarization camera is straight up toward the sky and can capture the underwater polarization patterns within Snell's window. GPS served as a reference for the polarization navigation information to verify the relevant position accuracy. We used the computer to control the ROV to dive at a specified depth and started to cruise at a designed route. The experimental target trajectory was a square with a side length of 40 m and a total length of 160 m. We collected the angle and position data every 10 m and the experiment trajectory at different depths

Fig. 8. Underwater DOP (a) and AOP (b) patterns at different time.

Fig. 9. Underwater DOP (a) and AOP (b) patterns at different depths.

are shown in Fig. 10. Then, we compared the measurement with the GPS and obtained the error of the method (Table 4). With depth increase, the errors of angle and position of underwater polarization navigation increase, which are consistent with the results of underwater polarization pattern. However, the practical trajectory is similar to the designed trajectory within this depth range and the precision can meet the real-time navigation requirements of UUV (Miller et al., 2010). The polarization navigation method is greatly affected by depth because the patterns are getting blurry with depth increase. It shows that underwater polarization navigation is feasible and has great potential within this depth range. As a new bionic visual navigation method, it exactly cannot work at much larger depths. But as photo-electric detection devices improve and underwater image enhancement technology develops, the polarization navigation will be able to work in deeper waters and plays a more important role. The results suggest that the underwater polarization pattern contains rich navigation information and can be used for navigation. However, many optical effects such as surface waves, water particles, and sea bottom reduce the performance of the method. In the future, the disturbance of multiple optical effects will be taken into consideration in the navigation model to improve the robustness and precision of the proposed method.
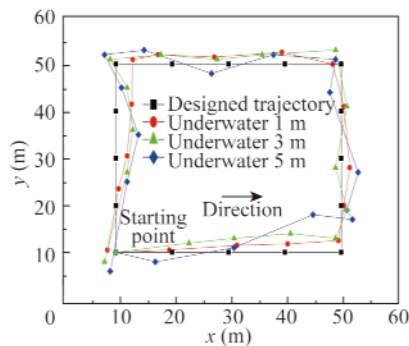

Fig. 10. ROV polarization navigation trajectory at different water depths.

Table 4 Tracking experiment error at different water depths

Depth (m)	Average angle error (°)	Average position error (m)
1	6.3333	2.0616
3	8.9757	3.2608
5	14.3508	4.0812

5 Conclusions

When UUV travels underwater, its navigation accuracy depends on the performance of the corresponding sensors. If the error is not corrected in time, it will lead to the continuous increase of heading and position errors, causing the UUV to deviate from the course and fail to complete the relevant task. Polarization navigation can provide accurate heading information for UUV and correct the heading error in time,

which can effectively improve the navigation accuracy of the underwater mission. As a biomimetic autonomous navigation method, it has the small volume, high accuracy, and better robustness for underwater operation. To better solve the underwater navigation problem with some new ideas, we propose a bioinspired underwater navigation method using polarization patterns within Snell's window in this paper. We establish the underwater polarized light transmission model and set up the detection device. By the simulation and experiment of underwater polarization patterns, we find that the AOP patterns within Snell's window are stable and can be used to determine the heading angle of UUV. In the water tank experiment, the average angle error of static and dynamic experiments is respectively 0.3954° and 0.8268°. In the real underwater environment, we conduct the navigation experiment at the depth of 1 m, 3 m, and 5 m. When the water depth is 5 m, the average angle and position error of the tracking experiment are 14.3508° and 4.0812 m, respectively. It is illustrated that polarization navigation is a feasible method that has the potential to be used in the water. The precision and robustness of the method will be improved if we conduct further calibration and such problems like that the effect of the unstable ocean current will be solved. The future study includes the improvement of the precision and experiment of other underwater environments.

Competing interests
The authors declare no competing interests.

References

Bok, M.J., Porter M. L., Place, A.R. and Cronin, T.W., 2014. Biological sunscreens tune polychromatic ultraviolet vision in mantis shrimp, *Current Biology*, 24(14), 1636–1642.

Browman, H.I. and Hawryshyn, C.W., 1994. The developmental trajectory of ultraviolet photosensitivity in rainbow trout is altered by thyroxine, *Vision Research*, 34(11), 1397–1406.

Cartron, L., Josef, N., Lerner, A., Mccusker, S.D., Darmaillacq, A.S., Dickel, L. and Shashar, N., 2013. Polarization vision can improve object detection in turbid waters by cuttlefish, *Journal of Experimental Marine Biology and Ecology*, 447, 80–85.

Cheng, H.Y., Chu, J.K., Zhang, R., Gui, X.Y. and Tian, L.B., 2020a. Real-time position and attitude estimation for homing and docking of an autonomous underwater vehicle based on bionic polarized optical guidance, *Journal of Ocean University of China*, 19(5), 1042–1050.

Cheng, H.Y., Chu, J.K., Zhang, R., Tian, L.B. and Gui, X.Y., 2020b. Underwater polarization patterns considering single Rayleigh scattering of water molecules, *International Journal of Remote Sensing*, 41(13), 4947–4962.

Cheng, H.Y., Chu, J.K., Zhang, R., Tian, L.B. and Gui, X.Y., 2020c. Turbid underwater polarization patterns considering multiple Mie scattering of suspended particles, *Photogrammetric Engineering & Remote Sensing*, 86(12), 737–743.

Cheng, H.Y., Chu, J.K., Zhang, R. and Zhang, P.Q., 2021a. Simulation and measurement of the effect of various factors on underwater polarization patterns, *Optik*, 237, 166637.

Cheng, H.Y., Wan, Z.H., Zhang, R. and Chu, J.K., 2021b. Visibility

improvement in turbid water by the fusion technology of Mueller matrix images, *International Conference on Artificial Intelligence and Computer Applications*, IEEE, Dalian, China.

Cox, C. and Munk, W., 1954. Measurement of the roughness of the sea surface from photographs of the sun's glitter, *Journal of the Optical Society of America*, 44(11), 838–850.

Dupeyroux, J., Viollet, S. and Serres, J.R., 2019. An ant-inspired celestial compass applied to autonomous outdoor robot navigation, *Robotics and Autonomous Systems*, 117, 40–56.

Gagnon, Y.L., Templin, R.M., How, M.J. and Marshall, N.K., 2015. Circularly polarized light as a communication signal in mantis shrimps, *Current Biology*, 25(23), 3074–3078.

Goddard, S.M. and Forward, R.B., 1991. The role of the underwater polarized light pattern, in sun compass navigation of the grass shrimp, *Palaemonetes vulgaris*, *Journal of Comparative Physiology A*, 169(4), 479–491.

Hawryshyn, C.W. and Bolger, A.E., 1990. Spatial orientation of trout to partially polarized light, *Journal of Comparative Physiology A*, 167(5), 691–697.

Horváth, G. and Varjú, D., 1995. Underwater refraction-polarization patterns of skylight perceived by aquatic animals through Snell's window of the flat water surface, *Vision Research*, 35(12), 1651–1666.

Huang, B.J., Liu, T.G., Hu, H.F., Han, J.H. and Yu, M.X., 2016. Underwater image recovery considering polarization effects of objects, *Optics Express*, 24(9), 9826–9838.

Ivanoff, A. and Waterman, T.H., 1958. Factors, mainly depth and wavelength, affecting the degree of underwater light polarization, *Journal of Marine Research*, 16, 283–307.

Liu, J., Hu, B.L., He, X.Q., Bai, Y., Tian, L.Q., Chen, T.Q., Wang, Y.H. and Pan, D.L., 2020. Importance of the parallel polarization radiance for estimating inorganic particle concentrations in turbid waters based on radiative transfer simulations, *International Journal of Remote Sensing*, 41(13), 4923–4946.

Lynch, D.K., 2015. Snell's window in wavy water, *Applied Optics*, 54(4), B8–B11.

Miller, P.A., Farrell, J.A., Zhao, Y.Y. and Djapic, V., 2010. Autonomous underwater vehicle navigation, *IEEE Journal of Oceanic Engineering*, 35(3), 663–678.

Parkyn, D.C., Austin, J.D. and Hawryshyn, C.W., 2003. Acquisition of polarized-light orientation in salmonids under laboratory conditions, *Animal Behaviour*, 65(5), 893–904.

Paull, L., Saeedi, S., Seto, M. and Li, H., 2014. AUV navigation and localization: A review, *IEEE Journal of Oceanic Engineering*, 39(1), 131–149.

Powell, S.B., Garnett, R., Marshall, J., Rizk, C. and Gruev, V., 2018. Bioinspired polarization vision enables underwater geolocalization, *Science Advances*, 4(4), eaao6841.

Sabbah, S., Barta, A., Gál, J., Horváth, G. and Shashar N., 2006. Experimental and theoretical study of skylight polarization transmitted through Snell's window of a flat water surface, *Journal of the Optical Society of America A*, 23(8), 1978–1988.

Shashar, N., Hagan, R., Boal, J.G. and Hanlon, R.T., 2000. Cuttlefish use polarization sensitivity in predation on silvery fish, *Vision Research*, 40(1), 71–75.

Shashar, N., Sabbah, S. and Cronin, T.W., 2004. Transmission of linearly polarized light in seawater: Implications for polarization signaling, *Journal of Experimental Biology*, 207(20), 3619–3628.

Stutters, L., Liu, H.H., Tiltman, C. and Brown, D.J., 2008. Navigation technologies for autonomous underwater vehicles, *IEEE Transactions on Systems, Man, and Cybernetics, Part C* (*Applications and Reviews*), 38(4), 581–589.

Tian, H., Zhu, J.P., Tan, S.W., Zhang, Y.Y., Zhang, Y., Li, Y.C. and Hou, X., 2018. Rapid underwater target enhancement method based on polarimetric imaging, *Optics & Laser Technology*, 108, 515–520.

Wang, Y.L., Chu, J.K., Zhang, R., Wang, L. and Wang, Z.W., 2015. A novel autonomous real-time position method based on polarized light and geomagnetic field, *Scientific Reports*, 5, 9725.

Waterman, T.H., 1955. Polarization of scattered sunlight in deep water, *Deep Sea Research*, 3(1), 426–434.

Waterman, T.H., 2006. Reviving a neglected celestial underwater polarization compass for aquatic animals, *Biological Reviews*, 81(1), 111–115.

Wu, T., Tao, C.H., Zhang, J.H. and Liu, C., 2018. Correction of tri-axial magnetometer interference caused by an autonomous underwater vehicle near-bottom platform, *Ocean Engineering*, 160, 68–77.

You, Y., Tonizzo, A., Gilerson, A.A., Cummings, M.E., Brady, P., Sullivan, J.M., Twardowski, M.S., Dierssen, H.M., Ahmed, S.A. and Kattawar, G.W., 2011. Measurements and simulations of polarization states of underwater light in clear oceanic waters, *Applied Optics*, 50(24), 4873–4893.

Zhang, R., Gui, X.Y., Cheng, H.Y. and Chu, J.K., 2021. Underwater image recovery utilizing polarimetric imaging based on neural networks, *Applied Optics*, 60(27), 8419–8425.

Zhang, Z., 2000. A flexible new technique for camera calibration, *IEEE Transactions on Pattern Analysis and Machine Intelligence*, 22(11), 1330–1334.

Zhou, G.H., Wang, J.W., Xu, W.J., Zhang, K. and Ma, Z.Q., 2017. Polarization patterns of transmitted celestial light under wavy water surfaces, *Remote Sensing*, 9(4), 324.